

NUMERICAL MODELLING OF VISCOPLASTIC FREE SURFACE FLOWS IN COMPLEX 3D GEOMETRIES

Kirill D. Nikitin¹, Maxim A. Olshanskii², Kirill M. Terekhov¹ and Yuri V. Vassilevski¹

¹Institute of Numerical Mathematics, Russian Academy of Sciences;
Moscow, Russia
e-mail: nikitin.kira@gmail.com, kirill.terehov@gmail.com, yuri.vassilevski@gmail.com

² Department of Mechanics and Mathematics, Moscow State University
Moscow, Russia
e-mail: Maxim.Olshanskii@mtu-net.ru

Keywords: free surface flows, viscoplastic fluid, Herschel-Bulkley fluids, adaptive mesh refinement, octree meshes

Abstract. *We study a numerical method for the simulation of free surface flows of viscoplastic (Herschel-Bulkley) fluids. The approach is based on the level set method for capturing the free surface evolution and on locally refined and dynamically adapted octree cartesian staggered grids for the discretization of fluid and level set equations. We consider an extension of the stable approximation of the Newtonian flow equations on staggered grid to approximate the viscoplastic model and level-set equations if the free boundary evolves and the mesh is dynamically refined or coarsened. In the Newtonian case, the convergence of numerical solutions is observed towards experimental data when the mesh is refined. We compute several viscoplastic Herschel-Bulkley fluid flows over incline planes for the dam-break problem. The comparison of numerical solutions is done versus experimental studies, indicating that intrinsically 3D numerical simulations are often required to compare well with a physical experiment. The efficacy of the numerical approach is demonstrated for a real-life application of landslide runout modelling in the Western Sayan mountains.*

1 INTRODUCTION

Free surfaces flows of yield stress fluids are common in nature: lava flows, snow avalanches and debris flows, as well as in engineering applications: flows of melt metal, fresh concrete, pastes and other concentrated suspensions [2, 26]. Although the rheology of such materials can be quite complicated, viscoplastic models, for example the Herschel-Bulkley model, are often used to describe the strain rate – stress tensor relationship and predict the fluids dynamics with reasonable accuracy, see e.g. [11, 18]. Modeling such phenomena numerically is a challenging task due to the non-trivial coupling of complex flow dynamics and free surface evolution.

Numerical simulations of viscoplastic fluid flow has already attracted a lot of attention, see, for example, the review papers [12, 15]. Nevertheless, the accurate modeling of *free-surface* viscoplastic fluid flows poses a serious challenge. The previous studies in this area include the application of the Arbitrary Lagrangian–Eulerian method for free-surface tracking of axisymmetric squeezing Bingham flows [21], volume of fluid surface tracking for 2D Bingham flows [1], the free interface lattice Boltzmann model [16], the simulation of viscoplastic fluids over incline planes in shallow layer approximations, see, e.g., [3, 5, 20].

The present paper reports on a numerical approach for simulation of complex 3D viscoplastic fluid flows. The approach is based on the free surface capturing by the level set method [34, 35] and octree cartesian grids dynamically refined near the free surfaces and coarsened in the fluid interior. The combination of the level set method and adaptive cartesian grids makes possible the efficient treatment of complex geometries emerging in the process of the free surface evolutions. We note that using grids adaptively refined towards a free boundary is a common practice, e.g. [7, 17]. Many adaptive methods studied in the literature are based on locally refined triangulations (tetrahedra) and finite element discretizations, e.g., [7, 14]. However, adaptive (octree) cartesian grids are more convenient for frequent and routine executions of refining / coarsening procedures. For the application of such grids in image processing, the visualization of amorphous medium, free surface Newtonian flow computations and other applications, where non-trivial geometries occur, see [23, 25, 27, 32, 36]. For the sake of adaptation, the grid is dynamically refined or coarsened according to the distance to the evolving free boundary on every time step. For the space discretization, we use a finite difference method with the staggered allocation of velocity–pressure nodes. A splitting scheme is applied for time integration.

The remainder of the paper is organized as follows. Section 2 reviews the mathematical model. In section 3 we discuss the details of the numerical approach. Numerical results for several 3D test problems are presented in section 4. Numerical tests include the viscoplastic Herschel-Bulkley fluid flow over incline planes and the simulation of a landslide runout in the Western Sayan mountains in vicinity of the Sayano-Shushenskaya dam. Section 5 contains some closing remarks.

2 MATHEMATICAL MODEL

We consider the Herschel-Bulkley model of a viscoplastic non-Newtonian incompressible fluid flow in a bounded time-dependent domain $\Omega(t) \in \mathbb{R}^3$. We assume that $\partial\Omega(t) = \overline{\Gamma_D} \cup \overline{\Gamma(t)}$, where Γ_D is the static boundary¹ (walls) and $\Gamma(t)$ is a free surface. In the time interval $(0, T]$,

¹The Γ_D part of the boundary may vary in time, although remaining static.

the fluid flow is described by the fluid equations

$$\begin{cases} \rho \left(\frac{\partial \mathbf{u}}{\partial t} + (\mathbf{u} \cdot \nabla) \mathbf{u} \right) - \operatorname{div} \boldsymbol{\tau} + \nabla p = \mathbf{f} \\ \nabla \cdot \mathbf{u} = 0 \end{cases} \quad \text{in } \Omega(t), \quad (1)$$

and the Herschel-Bulkley constitutive law

$$\begin{aligned} \boldsymbol{\tau} &= (K |\mathbf{D}\mathbf{u}|^{n-1} + \tau_s |\mathbf{D}\mathbf{u}|^{-1}) \mathbf{D}\mathbf{u} \Leftrightarrow |\boldsymbol{\tau}| > \tau_s, \\ \mathbf{D}\mathbf{u} &= \mathbf{0} \Leftrightarrow |\boldsymbol{\tau}| \leq \tau_s, \end{aligned} \quad (2)$$

where \mathbf{u} , p , $\boldsymbol{\tau}$ are velocity vector, pressure and the deviatoric part of the stress tensor, K is the consistency parameter, τ_s is the yield stress parameter, n is the flow index, for $n < 1$ the fluid is shear-thinning, for $n > 1$ is shear-thickening, and $n = 1$ corresponds to the classic case of the Bingham plastic, ρ is the density of fluid, $\mathbf{D}\mathbf{u} = \frac{1}{2}[\nabla \mathbf{u} + (\nabla \mathbf{u})^T]$ is the rate of strain tensor and $|\mathbf{D}\mathbf{u}| = \left(\sum_{1 \leq i, j \leq 3} |D_{ij} \mathbf{u}|^2 \right)^{\frac{1}{2}}$, div denotes the vector divergence operator. Thus the medium behaves like a fluid in the domain, where $|\mathbf{D}\mathbf{u}| \neq 0$, the so-called *flow region*, and exhibits the rigid body behavior in the region where the stresses do not exceed the threshold parameter τ_s , the so-called *rigid (or plug) region*. One of the difficult features of the problem is that two regions are unknown *a priori*. Since the stress tensor is indeterminate in the plug region, in [13] it was pointed out that (formally) the equations (1) make sense only on those parts of the domain, where $|\mathbf{D}\mathbf{u}| \neq 0$, and the mathematically sound formulation of (1)–(2) can be written in terms of variational inequalities. Another common way to avoid this difficulty in practice, is to regularize the problem by enforcing the fluidic medium behavior in the entire computational domain (see e.g. [6, 15]). We adopt this approach and replace $|\mathbf{D}\mathbf{u}|$ with $|\mathbf{D}\mathbf{u}|_\varepsilon = \sqrt{|\mathbf{D}\mathbf{u}|^2 + \varepsilon^2}$ for a *small* parameter $\varepsilon > 0$ (we set $\varepsilon = 10^{-7}$ in numerical experiments from this report). This allows us to pose equations in the entire domain:

$$\begin{cases} \rho \left(\frac{\partial \mathbf{u}}{\partial t} + (\mathbf{u} \cdot \nabla) \mathbf{u} \right) - \operatorname{div} \mu_\varepsilon \mathbf{D}\mathbf{u} + \nabla p = \mathbf{f} \\ \nabla \cdot \mathbf{u} = 0 \end{cases} \quad \text{in } \Omega(t), \quad (3)$$

with the shear-dependent effective viscosity

$$\mu_\varepsilon = K |\mathbf{D}\mathbf{u}|_\varepsilon^{n-1} + \tau_s |\mathbf{D}\mathbf{u}|_\varepsilon^{-1}.$$

At the initial time $t = 0$ the domain and the velocity field are known:

$$\Omega(0) = \Omega_0, \quad \mathbf{u}|_{t=0} = \mathbf{u}_0. \quad (4)$$

On the static part of the flow boundary we assume the Dirichlet (no-slip or inflow) or the Navier slip boundary conditions:

$$\mathbf{u} = \mathbf{g} \quad \text{on } \Gamma_D^1, \quad \mathbf{u} \cdot \mathbf{n} = \mathbf{n} \times [\mathbf{D}\mathbf{u}] \mathbf{n} = 0 \quad \text{on } \Gamma_D^2, \quad \Gamma_D^1 \cup \Gamma_D^2 = \Gamma_D, \quad (5)$$

here \mathbf{g} is given, \mathbf{n} is the normal vector to Γ_D . Balancing the surface tension and stress forces yields the second condition on $\Gamma(t)$:

$$\boldsymbol{\sigma}_\varepsilon \mathbf{n}_\Gamma = \zeta \kappa \mathbf{n}_\Gamma - p_{\text{ext}} \mathbf{n}_\Gamma \quad \text{on } \Gamma(t), \quad (6)$$

where $\boldsymbol{\sigma}_\varepsilon = \mu_\varepsilon \mathbf{D}\mathbf{u} - p \mathbf{I}$ is the regularized stress tensor of the fluid, κ is the sum of the principal curvatures, ς is the surface tension coefficient, p_{ext} is an exterior pressure which we assume to be zero, $p_{\text{ext}} = 0$.

The model of the free surface evolution uses the implicit definition of $\Gamma(t)$ as the zero level of a globally defined smooth (at least Lipschitz continuous) function $\phi(t, \mathbf{x})$,

$$\phi(t, \mathbf{x}) = \begin{cases} < 0 & \text{if } \mathbf{x} \in \Omega(t) \\ > 0 & \text{if } \mathbf{x} \in \mathbb{R}^3 \setminus \overline{\Omega(t)} \\ = 0 & \text{if } \mathbf{x} \in \Gamma(t) \end{cases} \quad \text{for all } t \in [0, T].$$

The initial condition (4) defines $\phi(0, \mathbf{x})$. For $t > 0$, the level set function satisfies the following transport equation [31]:

$$\frac{\partial \phi}{\partial t} + \tilde{\mathbf{u}} \cdot \nabla \phi = 0 \quad \text{in } \mathbb{R}^3 \times (0, T], \quad (7)$$

where $\tilde{\mathbf{u}}$ is any smooth velocity field such that $\tilde{\mathbf{u}} = \mathbf{u}$ on $\Gamma(t)$. The employed mathematical model consists of equations (3), (4), (5), (6), and (7). The implicit definition of $\Gamma(t)$ as the zero level of a globally defined function ϕ leads to numerical algorithms which can easily handle complex topological changes of the free surface such as merging or pinching of two fronts and formation of singularities. The level set function provides an easy access to useful geometric characteristics of $\Gamma(t)$. For instance, the unit outward normal to $\Gamma(t)$ is $\mathbf{n}_\Gamma = \nabla \phi / |\nabla \phi|$, and the surface curvature is $\kappa = \nabla \cdot \mathbf{n}_\Gamma$. From the numerical point of view, it is often beneficial if the level set function possesses the signed distance property, i.e., it satisfies the Eikonal equation

$$|\nabla \phi| = 1. \quad (8)$$

3 NUMERICAL METHOD

The numerical method is built on the approach developed in [27, 28] for the Newtonian flows and described in detail in [29, 30]. Below we outline the algorithm.

We apply a semi-implicit splitting method that avoids nested iteration loops and extends the well-known approach of Chorin-Temam-Yanenko, see, e.g., [9, 31]. Each time step of the method (given $\mathbf{u}(t), p(t), \phi(t)$ find approximations to $\mathbf{u}(t + \Delta t), p(t + \Delta t), \phi(t + \Delta t)$) consists of the following substeps. For the sake of presentation, we suppress spacial discretization details for a moment.

Level set part: $\Omega(t) \rightarrow \Omega(t + \Delta t)$.

1. Extend velocity to the exterior of fluid body: $\mathbf{u}(t)|_{\Omega(t)} \rightarrow \tilde{\mathbf{u}}(t)|_{\mathbb{R}^3}$. In practice, the extension is performed to a bulk computational domain, rather than \mathbb{R}^3 .
2. Find $\phi(t + \Delta t)$ from (7) by a numerical integration with the semi-Lagrangian method [37] and using the extended velocity field. This is done in few substeps: First, for every grid point \mathbf{y} , solve the characteristic equation backward in time

$$\frac{\partial \mathbf{x}(\tau)}{\partial \tau} = \tilde{\mathbf{u}}(\mathbf{x}(\tau), \tau), \quad \mathbf{x}(t + \Delta t) = \mathbf{y}, \quad \text{for } \tau \in [t + \Delta t, t]. \quad (9)$$

The characteristic equation is integrated numerically with the second order accuracy. Second, assign

$$\phi^*(\mathbf{y}, t + \Delta t) = \phi(\mathbf{x}(t), t). \quad (10)$$

To compute $\phi(\mathbf{x}(t), t)$ and velocity values along numerical characteristics, the second order interpolation is used. At this step, the signed distance property of ϕ and the volume balance may be lost.

3. Perform the correction $\phi^*(t + \Delta t) \rightarrow \widehat{\phi}^*(t + \Delta t)$ in order to enforce the global volume conservation;
4. Re-initialize the level set function $\widehat{\phi}^*(t + \Delta t) \rightarrow \phi(t + \Delta t)$ so that $\phi(t + \Delta t)$ (approximately) satisfies (8).

When the ‘‘level set’’ part of the splitting algorithm is complete, the computed $\phi(t + \Delta t)$ implicitly defines the new fluid domain $\Omega(t + \Delta t)$.

Remeshing. Given the new fluid domain we update and adapt the grid accounting for the new position of the free surface.

Re-interpolation. Further, all discrete variables are re-interpolated to the new grid. Note that the re-interpolated velocity field is defined globally (due to the extension procedure at the beginning of the level-set part).

Fluid part: $\{\mathbf{u}(t), p(t)\} \rightarrow \{\mathbf{u}(t + \Delta t), p(t + \Delta t)\}$.

1. First the advection is treated by applying the semi-Lagrangian method for each velocity component u_k , $k = 1, 2, 3$. This gives an intermediate velocity field $u_k^*(\mathbf{y}, t + \Delta t)$.
2. Next the viscoplastic terms are added:

$$\widehat{\mathbf{u}}^*(t + \Delta t) = \mathbf{u}^*(t + \Delta t) + \rho^{-1} \Delta t [\operatorname{div} (K |\mathbf{D}\tilde{\mathbf{u}}(t)|_\varepsilon^{n-1} + \tau_s |\mathbf{D}\tilde{\mathbf{u}}(t)|_\varepsilon^{-1}) \mathbf{D}\tilde{\mathbf{u}}(t) + \mathbf{f}(t)] \quad (11)$$

We split the surface tension balance condition (6) between the projection step (12) and the viscous step (11), so the velocity update in (11) uses the strain-free condition:

$$[\mathbf{D}\tilde{\mathbf{u}}(t)]_{\mathbf{n}_\Gamma}|_{\Gamma(t)} = 0$$

on the free boundary.

3. Solve for pressure $p(t + \Delta t)$:

$$\begin{cases} \nabla \cdot \nabla p(t + \Delta t) = \frac{1}{\Delta t} \nabla \cdot \widehat{\mathbf{u}}^*(t + \Delta t) & \text{in } \Omega(t + \Delta t), \\ p(t + \Delta t) = \rho^{-1} \varsigma \kappa(t + \Delta t) & \text{on } \Gamma(t + \Delta t) \quad \text{and} \quad \frac{\partial p(t + \Delta t)}{\partial \mathbf{n}} = 0 & \text{on } \Gamma_D. \end{cases} \quad (12)$$

Project the velocity on the div-free subspace:

$$\mathbf{u}(t + \Delta t) = \widehat{\mathbf{u}}^*(t + \Delta t) - \Delta t \nabla p(t + \Delta t).$$

Goto the level set part.

The time step is subject to the Courant type condition:

$$\Delta t = \min \left\{ C_1 h_{\min} \left(\max_{\mathbf{x} \in \Omega(t)} |\mathbf{u}(t)| \right)^{-1}, C_2 \rho^{\frac{1}{2}} h_{\min}^{\frac{3}{2}} \varsigma^{-\frac{1}{2}} \right\},$$

where h_{\min} is the size of the smallest volume cell as defined in the next section. In all computations we set $C_1 = 0.66$ and $C_2 = 1.4$, which were found sufficient for stability.

Note that we treat the viscoplastic terms explicitly in time. In this case, the standard stability analysis for parabolic equations would ask for the time step restriction $\Delta t \leq c h_{\min}^2 (\max \mu_\varepsilon)^{-1}$ (a prohibitively restrictive for $\max \mu_\varepsilon \gg 1$). However, such restriction was not found necessary in our computations. A possible explanation is that large effective viscosity values μ_ε correspond to a constrained fluid motion (tending to the rigid body motion) which resists to the development of spurious modes.

Resolving the geometry of the free surface and the accurate approximation of the surface tension forces require a sufficiently fine grid in a neighborhood of $\Gamma(t)$. In this case, the use of uniform grids becomes prohibitively expensive, especially in 3D. Locally refined meshes often need considerably less computational resources. However, such meshes have to be dynamically refined and coarsened if the free surface evolves. The remeshing is, in general, CPU time and memory demanding procedure for consistent regular tetrahedrizations. This step becomes considerably less expensive if one uses cartesian octree meshes with cubic cells. The two-dimensional analog of an octree mesh refined towards a 1D curve is illustrated in Figure 1 (left) and the midplane cut of an octree mesh in a numerical experiment of filling a container with a fluid is shown in Figure 1 (right). More details on quadtree/octree data structures can be found in [33].

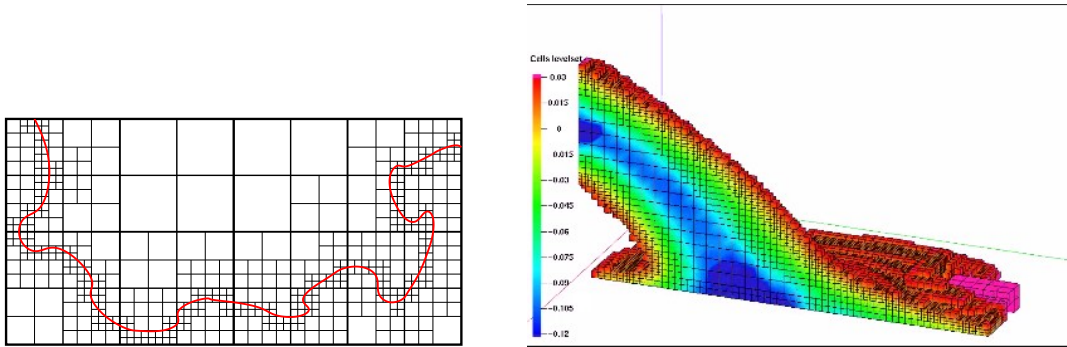


Figure 1: Left: 2D quadtree grid adapted to free boundary. Right: The midplane cut of an octree mesh, which is adaptively refined towards free surface in a numerical experiment of filling a container with a fluid.

For a stable finite difference method, we use the staggered location of velocity and pressure unknowns to discretize the fluid equations [19, 22]. The pressure is approximated in cell centers, velocity components are approximated in face centers. The level set function is approximated in cell vertices. Finite difference counterparts of the differential operators are considered in details in [29].

To account for the surface tension forces, we need approximations to the free surface normal vectors and curvatures. The unit outward normal vector is computed from the level set function: $\mathbf{n}_\Gamma = \nabla\phi/|\nabla\phi|$ on $\Gamma(t)$ by the second order approximation of the gradient. The mean curvature of the interface is defined as the divergence of the normal vector, $\kappa(\phi) = \nabla \cdot \mathbf{n} = \nabla \cdot (\nabla\phi/|\nabla\phi|)$. Since $\nabla\phi$ is computed with second order accuracy, $\kappa(\phi)$ is approximated at least with the first order.

The fluid volume is conserved globally by the regular adjustment of the level set function by adding a suitable constant function δ : $\phi^{new} = \phi - \delta$. The parameter δ solves the equation

$$\text{meas}\{\mathbf{x} : \phi(\mathbf{x}) < \delta\} = Vol^{\text{reference}}.$$

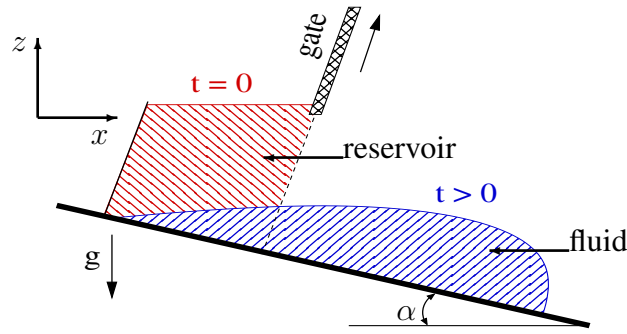


Figure 2: The sketch of the flow configuration used for Herschel-Bulkley fluid flow computations.

The bisection algorithm is used to find δ from this equation and a Monte-Carlo method is applied to evaluate $\text{meas}\{\mathbf{x} : \phi(\mathbf{x}) < \delta\}$.

Finally, we employ a re-initialization procedure defined in [28, 29] to satisfy the Eikonal equation (8) by the discrete level-set function.

4 NUMERICAL EXPERIMENTS

In this section we present results of several numerical tests. First, we validate the code by comparing computed statistics for the Newtonian case with those available in the literature. Further, few results are shown for viscoplastic fluid flows over incline planes and for landslide runout simulations.

4.1 The Herschel-Bulkley fluid flows over incline planes

Flows of viscoplastic fluids over incline surfaces have a long history in research due to their important role in nature and engineering, see [2, 20] for the review and the comprehensive coverage of the literature on the subject. Mathematical analysis of the problem, including the analytical representation of the form of the final arrested state, is available in the special case of two-dimensional shallow layer approximation and without inertia terms [3, 4, 5, 20]. Therefore, in a more general setting, numerical modeling is an important and indispensable research tool for analyzing such types of flows. Earlier numerical studies include computing the dam-break and sloping yield stress fluid flows in the shallow layer approximations (lubrication models), e.g. [3, 5, 20]. In such an approach, the effect of inertia and surface tension are often neglected. The method developed in this paper allows to account for true three-dimensionality of the flow as well as for inertia, surface tension, and more complex geometries, no shallow layer assumptions are needed.

First, the accuracy and the reliability of the method is demonstrated in [29], where for the case of the Newtonian fluid the convergence of the following statistic is shown to the experimental data found in a literature [24]. We computed the evolution of the free surface bottom front for the Newtonian dam break problem and compare it versus experimental values from [24]. When the finest grid size is of order $\frac{1}{256}$, then the computed results perfectly match the experiment. For non-Newtonian fluids, however, the existing models give typically less accurate approximation of a complex rheology of real-life fluids. Thus we look below for a qualitative comparison to experimental data (rather than the perfect matching).

Consider a plane inclined at angle α to the horizontal. A rectangular reservoir of length X and width Y filled with a volume V of Herschel-Bulkley fluid is placed on the plane. The

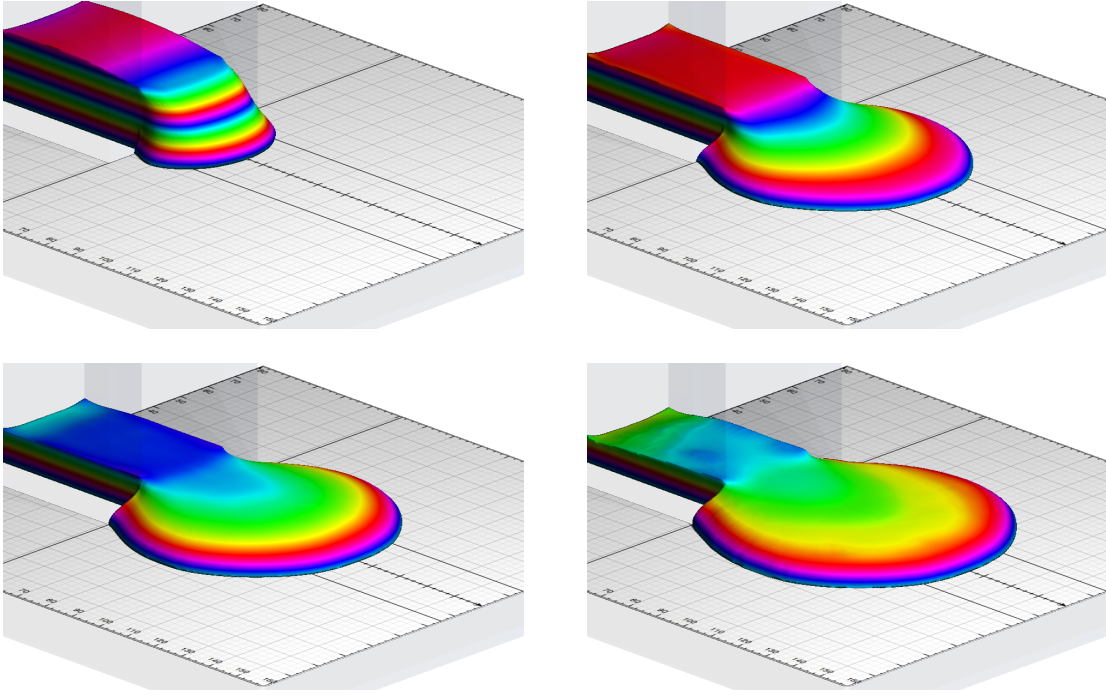


Figure 3: Three-dimensional view of the dam-break flow over incline plane with $\alpha = 12^\circ$ at times $t \in \{0.2, 0.6, 1.0, 2.0\}$ s with instantaneous gate removal and $K = 47.68 Pa s^{-n}$, $n = 0.415$, $\tau_s = 89 Pa$.

reservoir is equipped with a gate perpendicular to the slope. When the gate is open, the fluid is released and starts motion driven by the gravity force. The 2D schematic flow configuration is shown in Figure 2. The setup reproduces the experimental studies from [10].

We run numerical experiments with the following set of dimensional parameters from [10]: $X = 0.51m$, $Y = 0.3m$, $V = 0.06m^3$, $\alpha \in \{12^\circ, 18^\circ\}$, and two sets of Herschel-Bulkley model parameters, $K = 47.68 Pa s^{-n}$, $n = 0.415$, $\tau_s = 89 Pa$ and $K = 75.84 Pa s^{-n}$, $n = 0.579$, $\tau_s = 109 Pa$. The Herschel-Bulkley model with such parameters was found in [10] to approximate the rheology of Carbopol Ultrez 10 gel of 0.30% and 0.40% concentration, respectively. The gel has density $\rho = 937 kg/m^3$ and surface tension coefficient $\varsigma = 0.06 N/m$. The typical computed fluid evolution is illustrated in Figure 3, where the colors indicate the depth of the flow.

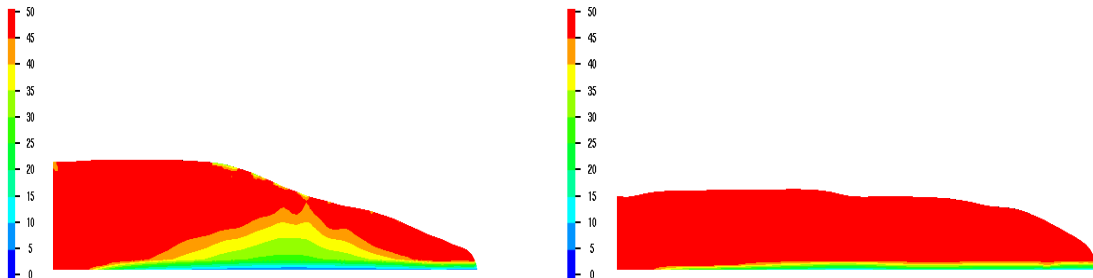


Figure 4: Effective viscosity μ_ε on midplane profile at times $t = 0.6s$ and $t = 1s$ for the same problem setup as in fig. 3.

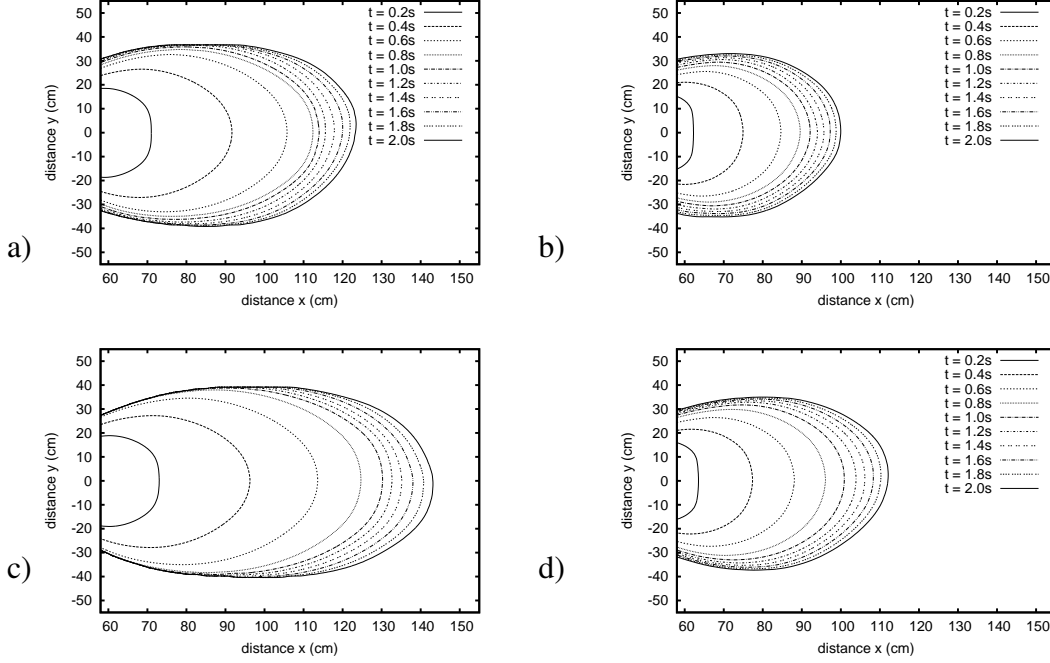


Figure 5: Contact line at times $t = 0.2k$ (s), $k = 1, \dots, 10$ for a) $\alpha = 12^\circ$, $K = 47.68 Pa s^{-n}$, $n = 0.415$, $\tau_s = 89 Pa$, b) $\alpha = 12^\circ$, $K = 75.84 Pa s^{-n}$, $n = 0.579$, $\tau_s = 109 Pa$, c) $\alpha = 18^\circ$, $K = 47.68 Pa s^{-n}$, $n = 0.415$, $\tau_s = 89 Pa$, d) $\alpha = 18^\circ$, $K = 75.84 Pa s^{-n}$, $n = 0.579$, $\tau_s = 109 Pa$.

Regarding the flow structure, the existing shallow-layer theory distinguishes the yielding region close to the bottom boundary and the pseudo-plug region, the region where the fluid is weakly yielded and considered solid up to higher order terms with respect to the layer thickness. Pseudo-plugs are predicted to dominate the dynamics over substantial regions of shallow flows. Qualitatively the same structure was observed for the computed 3D solutions and illustrated in figure 4.

We note that in the previous numerical studies of the dam-break problem, the whole bulk of fluid was assumed to be released instantaneously, i.e. the time needed for the gate to open was neglected. In the present approach, we are able to model the gradual removal of the gate as well. In [10] the gate was raised within $t = 0.8s$, which is not negligibly small time. Numerical results shown below were also computed for the gate gradually opened within $0.8s$. We found that without this detail the numerical solution (e.g., the flow-depth profile evolution) compared poorly to those found from experiment in [10]. Accounting for such effects is hardly possible if a numerical simulations use two-dimensional and/or shallow-layer models.

Figures 5 and 6 show the evolution of the contact line of the free-surface over the inclined plane and of the flow-depth profile at the midplane. We note that the fluid attains fast initial motion and sharply decelerates around $t = 0.8$. Further, the fluid front evolves gradually and slowly. Such two-stage behavior of numerical solution corresponds perfectly well to the experimental observations. In particular, describing the overall flow dynamics in experiments with Carbopol gel the authors of [10] stated “... we observed two regimes: at the very beginning ($t < 1s$), the flow was in an inertial regime; the front velocity was nearly constant. Then, quite abruptly, a pseudo-equilibrium regime occurred, for which the front velocity decayed as a power-law function of time.” Since we stop our simulation at $t = 2s$, we are not able to recover the asymptotic decay of the front velocity (the time scale of the real-life experiment was about 8 hours). Nevertheless, the computed contact line plots and midplane profiles (shown in Figures 5

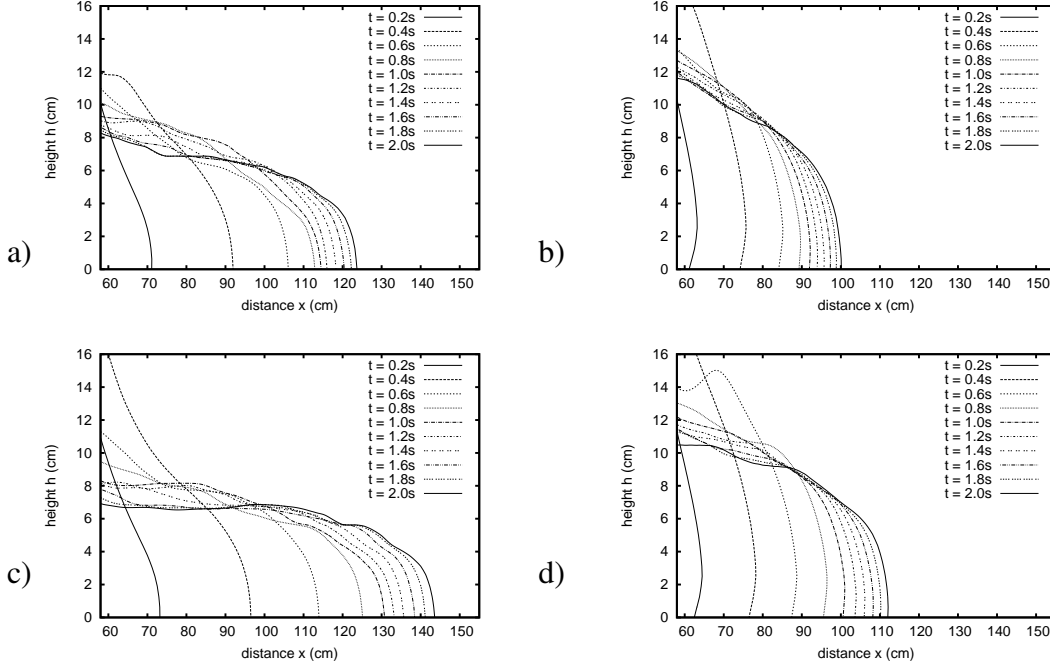


Figure 6: Midplane flow-depth profiles at times $t = 0.2k$ (s), $k = 1, \dots, 10$ for a) $\alpha = 12^\circ$, $K = 47.68 Pa s^{-n}$, $n = 0.415$, $\tau_s = 89 Pa$, b) $\alpha = 12^\circ$, $K = 75.84 Pa s^{-n}$, $n = 0.579$, $\tau_s = 109 Pa$, c) $\alpha = 18^\circ$, $K = 47.68 Pa s^{-n}$, $n = 0.415$, $\tau_s = 89 Pa$, d) $\alpha = 18^\circ$, $K = 75.84 Pa s^{-n}$, $n = 0.579$, $\tau_s = 109 Pa$.

and 6) compare well to the same statistics given in [10] for times $t \in \{0.2, 0.4, 0.6, 0.8, 1.0\}s$. In general, it should be noted that any viscoplastic model is an idealization of the possibly complex rheology of such fluid as Carbopol gel and certain deviation of numerical and experimental data is not unexpected.

4.2 Landslide runout modelling

As an example of the numerical simulation of a large-scale three-dimensional hydrodynamic event, we consider the modelling of a landslide runout in the Western Sayan mountains [30]. The calculations below do not correspond to any former accident or possible disaster scenario near the Sayano-Sushenskaya dam, but designed to show the feasibility of such calculations using the presented technology and if geophysical data for the coastal territory and the condition of the dam are available. For the computations we used a topographic map obtained from the Shuttle Radar Topography Mission (NASA) [38]. The accuracy of the map is about 90m. The polygonal approximation of the earth surface and the dam was constructed with the help of the Google SketchUp. We model a landslide runout on the left bank of the Yenisey river near the dam. Lacking a more accurate geophysical data, we take with the coefficients K , τ_s , n of the Herschel-Bulkley model from [8], which approximate the rheological properties of the grounds in the Puglia mountains in southern Italy.

When modeling a landslide, we were interested in the final deposition of masses and the pressure experienced by the body of the dam at the site of the landslide. The top view of the computed landslide runout at intermediate and final times is shown in Figure 7. The time variation of the total kinetic energy of the entire debris masses is shown in Figure 8, right. By the end of computation, the landslide has lost much of its kinetic energy and it is reasonable to assume that the final landslide deposition is found. The graph of maximum pressure on the body of the dam at the site of the landslide is shown in Figure 8, left. Due to the dynamic

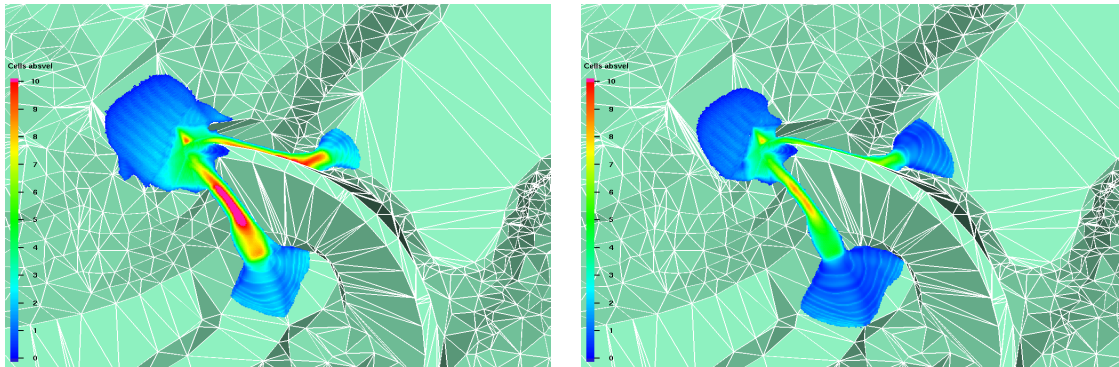


Figure 7: Landslide runout at times $t = 100\text{s}$ and $t = 167\text{s}$. Different colors show the absolute values of the velocity of landslide masses.

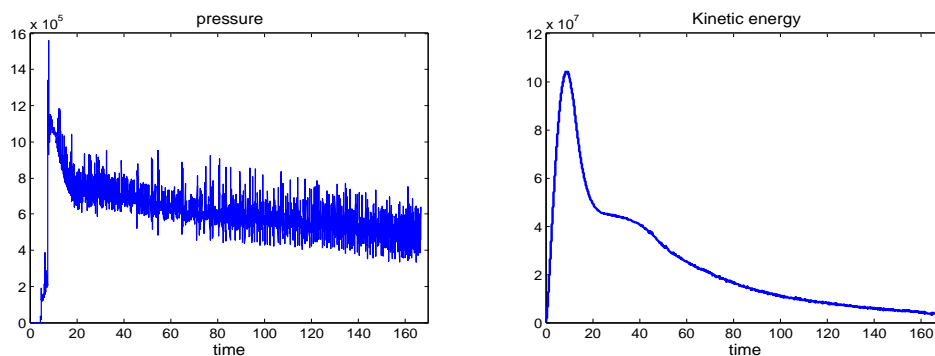


Figure 8: Pressure on the body of the dam at the site of the landslide. The change of kinetic energy of the entire landslide masses over time.

adaptivity, the maximum number of cubic cells in the present computations slightly exceeded 560 000. This leads to the algebraic problems of a modest size and makes the computations affordable on workstations or small clusters.

5 CONCLUSIONS

We considered a numerical method for computing free surface flows of viscoplastic fluids. The method is based on the level set function free surface capturing, on dynamically refined/coarsened octree cartesian grids, and semi-explicit splitting algorithm. It has been shown to be an efficient approach to simulate such types of flows numerically. We tested the performance of the method by computing several 3D viscoplastic fluid flows of interest. The computed viscoplastic solutions demonstrate expected qualitative behavior and compare reasonably well with experimental data.

Acknowledgments. This work has been supported in part by the Russian Foundation for the Basic Research grants 11-01-00971, 12-01-00283, 11-01-00767 and the federal programs “Scientific and scientific-pedagogical personnel of innovative Russia” and “Research and development in priority fields of S&T complex of Russia”

REFERENCES

- [1] A.N. Alexandrou, E. Duc, V. Entov, Inertial, viscous and yield stress effects in Bingham fluid filling of a 2D cavity, *J. Non-Newton. Fluid Mech.*, 96 (2001), 383–403.
- [2] C. Ancey, Plasticity and geophysical flows: a review, *J. Non-Newtonian Fluid Mech.*, 142 (2007), 4–35.
- [3] Ch. Ancey, S. Cochard, The dam-break problem for Herschel-Bulkley viscoplastic fluids down steep flumes, *J. Non-Newtonian Fluid Mech.*, 158 (2009), 18–35.
- [4] N.J. Balmforth, R.V. Craster, A consistent thin-layer theory for Bingham plastics, *J. Non-Newtonian Fluid Mech.*, 84 (1999), 65–81.
- [5] N. J. Balmforth, R. V. Craster, A. C. Rust, R. Sassi, Viscoplastic flow over an inclined surface, *J. Non-Newtonian Fluid Mech.*, 139 (2006), 103–127.
- [6] M. Bercovier and M. Engelman, A finite element method for incompressible non-Newtonian flows, *J. Comp. Phys.*, 36 (1980), pp. 313–326.
- [7] E. Bertakis, S. Gross, J. Grande, O. Fortmeier, A. Reusken, A. Pfennig, Validated simulation of droplet sedimentation with finite-element and level-set methods, *Chem. Eng. Science*, 65 (2010), 2037–2051.
- [8] T. Bisantino, P. Fischer, F. Gentile, Rheological characteristics of debris-flow material in South-Gargano watersheds, *Nat Hazards*, 54 (2010), 209–223.
- [9] A. Chorin, Numerical solution of the Navier-Stokes equations. *Math. Comp.*, 22 (1968), 745–762.
- [10] S. Cochard, C. Ancey, Experimental investigation of the spreading of viscoplastic fluids on inclined planes, *J. Non-Newtonian Fluid Mech.*, 158 (2009), 73–84.
- [11] P. Coussot, *Mudflow Rheology and Dynamics*, Balkema, Rotterdam, 1997.
- [12] E. J. Dean, R. Glowinski, G. Guidoboni, On the numerical simulation of Bingham viscoplastic flow: Old and new results, *J. Non-Newtonian Fluid Mech.*, 142 (2007), 36–62.
- [13] G. Duvaut and J. L. Lions, *Inequalities in Mechanics and Physics*, Springer, 1976.
- [14] P. Esser, J. Grande, A. Reusken, An extended finite element method applied to levitated droplet problems, *Int. J. for Numer. Meth. in Engineering*, (2010). DOI: 10.1002/nme.2913
- [15] I.A.Frigaard, C.Nouar, On the usage of viscosity regularization methods for viscoplastic fluid flow computation, *J. Non-Newtonian Fluid Mech.*, 127 (2005), 1–26.
- [16] I. Ginzburg, K. Steiner, A free-surface lattice Boltzmann method for modelling the filling of expanding cavities by Bingham fluids, *Phil. Trans. R. Soc. Lond. A*, 360 (2002), 453–466.
- [17] I. Ginzburg, G. Wittum, Two-phase flows on interface refined grids modeled with VOF, staggered finite volumes, and spline interpolants, *J. Comput. Phys.*, 166 (2001), 302–335.

- [18] R.W. Griffiths, The dynamics of lava flows, *Annu. Rev. Fluid Mech.*, 32 (2000), 477–518.
- [19] F. Harlow, J. Welch. Numerical calculation of time-dependent viscous incompressible flow of fluid with free surface. *Phys. Fluids*, 8 (1965), 2182-2189.
- [20] A.J. Hogg, G.P. Matson, Slumps of viscoplastic fluids on slopes, *J. Non-Newtonian Fluid Mech.*, 158 (2009), 101–112.
- [21] G. Karapetsas, J. Tsamopoulos, Transient squeeze flow of viscoplastic materials, *J. Non-Newtonian Fluid Mech.*, 133 (2006), 35–56.
- [22] V. Lebedev, Difference analogues of orthogonal decompositions, basic differential operators and some boundary problems of mathematical physics, I,II. *U.S.S.R. Comput. Math. Math. Phys.*, 4(3) (1964), 69–92, 4(4) (1964), 36–50.
- [23] F. Losasso, F. Gibou, R. Fedkiw, Simulating water and smoke with an octree data structure, *ACM Transactions on Graphics (TOG)*, 23 n.3, August 2004.
- [24] J. Martin, W. Moyce, An experimental study of the collapse of liquid columns on a rigid horizontal plane, *Philos.Trans.R.Soc.Lond.Ser.A*, 244 (1952), 312–324.
- [25] C. Min, F. Gibou, A second order accurate level set method on non-graded adaptive cartesian grids, *J. Comput. Phys.*, 225 (2007), 300–321.
- [26] Q.D. Nguyen, D.V. Boger, Measuring the flow properties of yield stress fluids, *Annu. Rev. Fluid Mech.*, 24 (1992), 47–88.
- [27] K.D. Nikitin, Y. V. Vassilevski, Free surface flow modelling on dynamically refined hexahedral meshes, *Rus. J. Numer. Anal. Math. Model.*, 23 (2008) 469–485.
- [28] K.D. Nikitin, M.A. Olshanskii, K.M. Terekhov, Y. V. Vassilevski, Numerical simulations of free surface flows on adaptive cartesian grids with level set function method, *Report is available online*, 2010.
- [29] K.D. Nikitin, M.A. Olshanskii, K.M. Terekhov, Y. V. Vassilevski, A numerical method for the simulation of free surface flows of viscoplastic fluid in 3D, *J. Comp. Math.*, V. 29 (2011) 605–622.
- [30] K.D. Nikitin, M.A. Olshanskii, K.M. Terekhov, Y. V. Vassilevski, CFD technology for 3D modelling of large scale hydrodynamic events and catastrophes, to appear in *Rus. J. Numer. Anal. Math. Model.*.
- [31] S. Osher, R. Fedkiw, *Level Set Methods and Dynamic Implicit Surfaces*. Springer-Verlag, 2002.
- [32] S. Popinet, An accurate adaptive solver for surface-tension-driven interfacial flows, *J. Comput. Phys.*, 228 (2009), 5838–5866.
- [33] H. Samet, *The Design and Analysis of Spatial Data Structures*, Addison-Wesley, New York, 1989.
- [34] R. Scardovelli, S. Zaleski, Direct numerical simulation of free-surface and interfacial flow, *Annual Review of Fluid Mechanics*, 31 (1999), 567–603.

- [35] J.A. Sethian, *Level Set Methods and Fast Marching Methods: Evolving Interfaces in Computational Geometry, Fluid Mechanics, Computer Vision, and Materials Science*, Cambridge University Press, Cambridge, 1999.
- [36] J. Strain, Tree Methods for Moving Interfaces, *J. Comput. Phys.*, 151 (1999), 616–648.
- [37] J.Strain, Semi-Lagrangian methods for level set equations. *J. Comput. Phys.*, 151 (1999), 498–533.
- [38] <http://www2.jpl.nasa.gov/srtm/>